
Rare earth elements as new biogeochemical proxies in deep-sea mussels

Barrat Jean-Alix ^{1,2,*}, Bayon Germain ³, Carney Robert S. ⁴, Chauvaud Laurent ¹

¹ Univ Brest, CNRS, LEMAR, Institut Universitaire Européen de la Mer (IUEM), Place Nicolas Copernic, 29280 Plouzané, France

² Institut Universitaire de France, France

³ Univ Brest, CNRS, Ifremer, Geo-Ocean, F-29280 Plouzané, France

⁴ Department of Oceanography and Coastal Sciences, Louisiana State University, Baton Rouge, LA 70803, USA

* Corresponding author : Jean-Alix Barrat, email address : barrat@univ-brest.fr

Abstract :

We report on the abundances of REE in a comprehensive suite of shells of deep-sea chemosynthetic mussels from hydrothermal vents and cold seeps. Except for mussel shells from oceanic hydrothermal sites that often show extremely pronounced Eu anomalies ($(\text{Eu}/\text{Sm})_{\text{sn}} = 2\text{--}200$), and abundances for this element that can occasionally exceed 200 ng/g, REE concentrations are usually low and typically between $10\text{--}4$ and $10\text{--}3$ times the shale reference.

In addition to exhibiting commonly high Eu anomalies, mussel shells from hydrothermal vents are depleted in light-REE and heavy-REE compared to reference shales (e.g., $(\text{Pr}/\text{Sm})_{\text{sn}} < 1$, $(\text{Tb}/\text{Yb})_{\text{sn}} = 1\text{--}6$). These features are inherited from hydrothermal fluid. Mussel shells from cold seeps have very different REE concentrations, which also reflect the compositions of the waters they filter: their $(\text{Eu}/\text{Sm})_{\text{sn}}$ ratios are much lower (< 2) and are much less heavy-REE fractionated ($(\text{Tb}/\text{Yb})_{\text{sn}} = 0.5\text{--}2.7$). Furthermore, the REE distributions show a clear dichotomy between thiotrophic and methanotrophic mussels. The latter show marked enrichments in light-REE and even sometimes La enrichments much larger than those classically observed in deep-sea waters, leading to huge positive La anomalies ($\text{La}/\text{La}^* > 10$). These light-REE enrichments are likely related to REE-dependent methanol dehydrogenase enzymes used by the symbionts that these mussels host in their gills. These data show that REE chemistry is a promising tool to study chemosynthetic faunas living near hydrothermal vents or cold seeps. Furthermore, REE chemistry, coupled with stable isotopes, should reveal the footprint of aerobic methanotrophy in carbonates formed in cold seeps, but also potentially in ancient sediments.

Highlights

► Mussel shells from hydrothermal vents show large Eu anomalies. ► REE patterns of thiotrophic and methanotrophic mussel shells are different. ► Shells of methanotrophic mussels exhibit distinctive LREE enrichments and often, large positive La anomalies. ► REE chemistry is a promising tool to study chemosynthetic faunas.

Keywords : Rare earth elements, Bivalve, Shell chemistry, Hydrothermal system, Cold seep, Methanotrophy

55 **1/ Introduction**

56 Over the last fifty years, rare earth elements (REEs) have become one of the most
57 studied groups of elements by geochemists, finding applications in all fields, from the
58 petrogenesis of rocks, terrestrial or not, to the origin of the first condensed solids in the solar
59 system, through rock dating and isotope tracing (e.g., Henderson, 1984). In marine
60 geochemistry, REEs and their isotopes have been also extensively studied since they allow,
61 among other things, the characterization of the different water masses composing the oceans
62 and their circulation (e.g., Elderfield, 1988). For decades, it has been assumed that these
63 elements do not participate in any biochemical cycle and therefore that their distributions at
64 the Earth's surface are not impacted by life. Nature is certainly more complex. Notable
65 biological effects of the REEs have been observed in plants, and REEs are even used as
66 fertilizers (Tommasi et al., 2021). Furthermore, some species can accumulate large amounts
67 of these elements, as exemplified by the fern *Dicranopteris linearis* (Ozaki et al., 1997). More
68 recently, it was established that light REEs are vital for aerobic methanotrophic and
69 methylotrophic bacteria that play an essential role in global carbon cycling (e.g., Pol et al.,
70 2014; Semrau et al., 2018; Cotruvo, 2019). Methanotrophic bacteria first convert methane to
71 methanol, which is subsequently degraded into formaldehyde using Ca-dependent (MxaF
72 type) or REE-dependent (XoxF type) methanol dehydrogenase enzymes (Skovran *et al.*,
73 2011). Ramachandran and Walsh (2015) and Taubert et al. (2015) have shown that XoxF type
74 enzymes are more frequently used by marine bacteria. These recent findings clearly indicate
75 the ability of micro-organisms to fractionate and redistribute REE, emphasizing the
76 importance of life in the REE cycling in Earth's surface environments. For instance, there is
77 growing evidence that bacterial activity and chemosynthetic ecosystems can influence the
78 REEs distribution in seawater, at least locally. During the blowout of the Deepwater Horizon
79 well (Gulf of Mexico), the depletion of light REE in a submerged plume of methane-rich
80 water was explained by an uptake of these elements by methanotrophic bacteria (Shiller et al.,
81 2017). More recently, light REE depletions were observed in seawater from the Sargasso Sea,
82 at depths between approximately 200 and 500 m, ascribed to the activity of methanotrophic or
83 methylotrophic microorganisms (Meyer et al., 2021). Therefore, methanotrophic bacteria, at
84 least those using enzymes containing REEs, display distinctive REE distributions, as do
85 animals living in symbiosis with them.

86 Within this scope, deep-sea fauna associated with black smokers and cold seeps are
87 ideal targets to evaluate the distinctive chemical signatures developed by organisms. In these
88 environments, reduced sulfur compounds, methane and/or hydrogen fuel primary productivity
89 sustained by the symbiotic bacteria that form here the basis of the trophic web (Cavanaugh et
90 al., 1981, 1987; Felbeck, 1981; Childress et al., 1986; Petersen et al., 2011), which are vital
91 for many thiotrophic or methanotrophic animals. Recently, two investigations of
92 chemosynthetic fauna have provided direct support for an active consumption of light-REE
93 associated with aerobic microbial oxidation of methane at cold seeps. Bayon et al. (2020a)
94 determined trace element abundances along a one-meter-long chitin tube of a siboglinid worm
95 (*Escarpia southwardae*) collected at the Regab pockmark (Congo margin), identifying
96 distinctive light REE enrichments that were attributed to methanotrophic activity in the
97 branchial plume region of the worm. Additionally, similar light-REE enrichments were found
98 in the gills of methanotrophic mussels collected at seeps from the South China Sea, but not in
99 thiotrophic clams or mussels from the same sites (Wang et al., 2020). Because gills are the
100 organs hosting the methanotrophic symbionts in mussels, Wang et al. (2020) proposed that
101 these light-REE enrichments were related to aerobic methanotrophy. In that latter study, other
102 soft tissues and the shell of studied methanotrophic mussels, while displaying lower light-
103 REE abundances, also show higher positive La anomalies relative to seawater or pore water.

104 Rare earth element data for deep-sea shells are still sparse. To date, mussels from only
105 three hydrothermal vent fields (Bau et al., 2010) and two cold seeps (Wang et al., 2020) have
106 been investigated. Here we present a comprehensive review for the distribution of REE in
107 mussel shells from deep-sea chemosynthetic environments, which combine previously
108 published literature data (Bau et al., 2010; Wang et al., 2020) and new results obtained on a
109 suite of deep-sea mussels from both submarine methane seeps and hydrothermal vents (Fig.
110 1). The aim of this study was to further investigate the factors influencing the REE
111 distribution in marine mollusks and assess the degree to which REE abundances in shells can
112 be used to monitor the activity of methanotrophic symbiotic bacteria.

113

114 **2/ Sampling**

115 Forty-five mussel shells belonging to ten different species were analyzed here, of
116 which nine reside in the genus *Bathymodiolus*. Application of DNA analyses to newly
117 discovered species has led to the assignment of the intensively studied *Bathymodiolus*

118 *childressi* to the genus *Gigantidas* (Xu et al., 2019). Twenty-five shell samples, belonging to
119 nine species of *Bathymodiolus*, were sourced from the Scripps Institution of Oceanography
120 Benthic Invertebrate Collection (SIO-BIC) in La Jolla (California, USA). Our sampling
121 includes both thiotrophic and methanotrophic species. Descriptive data for each sample (site,
122 depth, species, museum catalog number, etc.) are given in Supplementary Table 1.

123

124 **2.1/ Hydrothermal vents**

125 We analyzed three shells from three different sites in the Pacific Ocean for this study,
126 which complement the dataset obtained by Bau et al. (2010) on thiotrophic mussels from the
127 Mid-Atlantic Ridge. Two mussels (*Bathymodiolus thermophilus*) originate from the East
128 Pacific Rise (SIO-BIC M16462) and the Rose Garden vent field (SIO-BIC M8223) located
129 east of the Galápagos Islands, which was among the first submarine hydrothermal sites
130 discovered (e.g., Corliss and Ballard, 1977). The third shell (*Bathymodiolus septemdierum*;
131 SIO-BIC M15353) comes from the Nifonea vent field (Schmidt et al., 2017), located within
132 the caldera of a large shield-type volcano of the Vate Trough, a young extensional rift in the
133 New Hebrides back-arc (Vanuatu, SW Pacific).

134

135 **2.2/ Cold seeps**

136 We analyzed samples from seven seeps located in three different regions: the Gulf of
137 Mexico, the western margin of Costa Rica, and Melanesia.

138 The Gulf of Mexico seeps (Brine Pool, Bush Hill, and West Florida Escarpment) have
139 been extensively studied both geologically and biologically (Paull et al., 1984, 1985; Martens
140 et al. 1991; Chanton et al., 1993), and were the basis for seminal observations on
141 chemoautrophic life, including the demonstration of methane-based symbiosis between
142 animals and intracellular bacteria (Childress et al., 1986). The mussels of these sites are
143 particularly well characterized, and the reader is referred to the numerous papers concerning
144 in particular their symbionts or their isotopic compositions allowing analysis of their diet
145 (e.g., Duperron et al., 2007; Macavoy et al., 2008; Riekenberg et al., 2018; Feng et al., 2018).
146 Twenty *Gigantidas childressi* shells from Brine Pool and Bush Hill, and one *Bathymodiolus*
147 *heckerae* shell from West Florida Escarpment (SIO-BIC M8018), were analyzed. *Gigantidas*
148 *childressi* is associated with only one type of methanotrophic symbionts, and consumes
149 primarily methane. The metabolism of *Bathylomodius heckerae*, predominantly

150 methanotrophic, is however potentially much more complex as its gills harbor a greater
151 diversity of symbionts, including one methanotrophic, one methylotrophic, and two
152 thiotrophic polytypes (Duperron et al., 2007). However, $\delta^{13}\text{C}$ values of these mussels confirm
153 that seep hydrocarbons represent the dominant carbon source in their soft tissues (Cavanaugh
154 et al., 1987; Paull et al., 1989; Duperron et al., 2007).

155
156 Cold seeps at the continental margin offshore Costa Rica harbor a varied fauna
157 (Sahling et al., 2008; Levin et al., 2012, 2015), including mytilid species whose distribution
158 shows some stratification with water depth (McCowin et al., 2020): *Bathymodiolus*
159 *billschneideri* (~1400–1900 m), *B. earlougheri* (~1000–1900 m), and *B. nancyschneiderae*
160 (1000–1100 m). Furthermore, *Bathymodiolus thermophilus*, a thiotrophic mussel typically
161 encountered at hydrothermal vents along the Galápagos Rift Zone and the East Pacific Rise
162 (e.g., Kenk and Wilson, 1985), has been also identified in this area (McCowin et al., 2020).
163 These four species are all thiotrophic (Levin et al., 2012; Brzechffa and Goffredi, 2021). A
164 total of twenty shells from three seeps (Jaco Scar, Mound 12, and Parrita Seep) were analyzed
165 (SIO-BIC specimens listed in Table S-1).

166 Two mussel shells (*Bathymodiolus edisonensis*, SIO-BIC M18361; and *B.*
167 *anteumbonatus*, SIO-BIC M15360) from a cold seep in the vicinity of Edison Seamount (New
168 Ireland Basin, Melanesia, Herzig et al., 1998) complement our sampling of methane seep
169 mollusks. Mussels from this location have been described by von Cosei and Janssen (2008),
170 but to the best of our knowledge, the nature of their symbionts and their isotopic compositions
171 are unknown. The abundance of methane at these sites (Herzig et al., 1998), as well as the
172 similarities of these shells to *Gigantidas childressi* from Gulf of Mexico, strongly suggest that
173 they are methanotrophic (von Cosei and Janssen, 2008).

174

175 **3/ Analytical procedures**

176 Periostracum was removed from the shells by scraping using a clean steel blade. The
177 determination of the REE abundances follows the procedure designed by Barrat et al. (2020).
178 About 150–200 mg of shell were precisely weighted, spiked with Tm, and dissolved with
179 HNO_3 . REE and Y were separated using ion-exchange chromatographic columns loaded with
180 about 1 ml DGA resin. The measurements were performed on a Thermo Scientific
181 ELEMENT XR™ spectrometer located at the “Pôle Spectrométrie Ocean”, Institut

182 Universitaire Européen de la Mer (IUEM), Plouzané (France). The reader is referred to
183 previous papers where our analytical methodology for carbonate samples (Barrat et al., 2020),
184 calibration, isobaric interference corrections and calculation of concentrations based on Tm
185 addition are extensively described, and in which reference values for many international rock
186 standards are reported (e.g., Barrat et al., 1996, 2012, 2016; Charles et al., 2021).

187 Measured REE concentrations were normalized to the Post Archean Australian Shale
188 (PAAS; Pourmand et al., 2012), adjusted to standard results obtained in our laboratory (Barrat
189 et al., 2020). The La, Ce, and Gd anomalies were calculated using the La/La^* , Ce/Ce^* ,
190 Gd/Gd^* ratios, where X^* is the extrapolated concentration for a smooth PAAS-normalized
191 REE pattern and X_{sn} is the concentration of element X normalized to PAAS: $La_{sn}^* =$
192 Pr_{sn}^3/Nd_{sn}^2 , $Ce_{sn}^* = Pr_{sn}^2/Nd_{sn}$, $Gd_{sn}^* = Tb_{sn}^2/Dy_{sn}$. Replicate measurements obtained for two
193 carbonate standards (CAL-S and BEAN) during the analytical sessions are given in
194 Supplementary Table 1, together with reference values from the literature. The precision
195 (RSD) on measured abundances and elemental ratios was generally better than 3 %. Note that
196 there is no analytical bias between the REE concentrations presented here and those obtained
197 by Wang et al. (2020), which were obtained using the same procedure in our laboratory; or
198 those from Bau et al. (2010) obtained at Jacobs University (Bremen), which are also of very
199 high quality. However, Y concentrations obtained in Bremen on different standards (e.g., Bau
200 et al., 2010, 2014, 2018) were systematically lower than those obtained in Brest (e.g., Barrat
201 et al., 2012, 2020, Charles et al., 2021). This calibration bias was corrected here by
202 multiplying all Y concentrations obtained by Bau et al. (2010) by 1.10.

203

204 **4/ Results**

205 Sixty-six shell analyses were obtained here (supplementary Table 1), greatly
206 increasing the number of available data for deep-sea mussels. These shells are very poor in
207 REEs. Only rarely did concentrations of an element exceed 100 or 200 ng/g (e.g. Eu for some
208 samples from hydrothermal vents). PAAS-normalized REY patterns from the available data
209 set (Bau et al., 2010; Wang et al., 2020 and this work) are given in Figures 2-5 and provide an
210 overview of the diversity of compositions of these shells.

211

212

213

214 **4.1/ Hydrothermal vent mussels**

215 As shown by Bau et al. (2010), the shells of hydrothermal vent mussels have REY
216 patterns showing large positive Eu anomalies, inherited from hydrothermal fluids (Fig. 2). In
217 this regard, the shells analyzed here are no exception. The East Pacific shells show identical
218 patterns (Fig. 2b), except for Eu, with the EPR sample having an Eu-anomaly similar to those
219 from Logatchev (Fig. 2a) and the Rose Garden sample similar to those from Golden Valley
220 (Fig. 2c) obtained by Bau et al. (2010). Both samples are also marked by positive Y and
221 negative Ce anomalies that are unquestionably the fingerprint of seawater. Two samples of
222 the same shell from Nifonea were analyzed and the results are almost identical, suggesting a
223 homogeneity of the latter (Fig. 2e). The patterns obtained show positive Eu anomalies lower
224 than for the two other samples from Pacific, as well as negative anomalies in Ce and positive
225 in Y quite pronounced. These patterns are similar to those of Lilliput (Fig. 2b). The less
226 pronounced Eu anomalies here could be explained by the composition of hydrothermal fluids,
227 whose Eu anomalies are much lower than those of typical oceanic hydrothermal fluids
228 (Schmidt et al., 2017), but also by a more important contribution of ambient seawater than for
229 the other sites.

230

231 **4.2/ Cold seep mussels**

232 **4.2.1/ Thiotrophic mussels**

233 Only three thiotrophic mussel shells from the China Sea (Site F, Fig. 1) had been
234 analyzed before this study (Wang et al., 2020). Here we studied a much larger series of such
235 mussels collected from three sites located in western Costa Rica. Four species of mussels
236 were analyzed. For these three sites, whatever the species considered, the REY-patterns are
237 quite similar (Fig. 3), and comparable in abundance and shape to those of *Bathymodiolus*
238 *aduloides* collected in the China Sea (Fig. 4 b). Unlike shells from hydrothermal sites, these
239 shells display low $(\text{Eu}/\text{Sm})_{\text{sn}}$ ratios (=1.21-1.92). The shape of their REY patterns resembles
240 those of marine carbonates (e.g., Northdurft et al., 2004). The patterns are characterized by
241 marked negative Ce anomalies ($\text{Ce}/\text{Ce}^*= 0.34\text{-}0.77$ for Costa Rica samples, and $0.77\text{-}0.81$ for
242 China Sea samples) and positive Y anomalies ($\text{Y}/\text{Ho}= 51\text{-}80$ for Costa Rica samples, and 50-
243 64 for China Sea samples). They also display positive anomalies in La ($\text{La}/\text{La}^*=1.9\text{-}3.0$) in
244 the range of seawater values, and apparent positive anomalies in Gd ($\text{Gd}/\text{Gd}^*=1.1\text{-}1.37$).

245

246 **4.2.1/ Methanotrophic mussels**

247 The two *Bathymodiolus* shells from the Edison Seamount display lower REE than the
248 *Gigantidas* from the China Sea (Wang et al., 2020), but their patterns show quite similar
249 characteristics (Fig. 4). Two fragments per shell were analyzed, and the results are very
250 consistent, suggesting that both shells do not show marked heterogeneities for REE and Y. As
251 expected, they show positive anomalies in Y ($Y/Ho=59.8-69.5$) and negative in Ce
252 ($Ce/Ce^*=0.39-0.46$), but also striking La anomalies ($La/La^*=7.9-11.9$). Wang et al. (2020)
253 previously showed that the shells of methanotrophic mussels from the China Sea display
254 exceptionally high positive anomalies in La ($La/La^*=2.5-5.1$). Those measured in Edison
255 Seamount shells are even higher, and to the best of our knowledge, represent the most
256 pronounced La anomalies ever measured to date in natural environments not affected by
257 emerging micropollutants. In addition, these shells also show apparent anomalies in Gd
258 ($Gd/Gd^*=1.26-1.77$).

259 Different REY patterns were obtained for mussels from the Gulf of Mexico (Fig. 5):

260 -The patterns of *Gigantidas* shells from Brine Pool and Bush Hill show distinctive
261 light REE enrichments, moderate negative Ce anomalies, variable Gd anomalies
262 ($Gd/Gd^*=0.88-1.53$), as well as usual seawater-like positive Y anomalies ($Y/Ho=43.8-72.5$).
263 Their La anomalies ($La/La^*=1.73-2.70$) are not as high as those discussed above, being
264 comparable to typical marine values. Mussels from these two sites display similar REE
265 concentrations, showing that the brines at Brine Pool do not affect the REE composition of
266 shells. Note that the mussels at this site do not live in direct contact with the brines but within
267 at ~10-cm-thick layer of seawater immediately overlying the brine pool or the surficial
268 sediment at the pool edge. However, a sample from Brine Pool (BP7a) stands out from other
269 shells by displaying higher heavy REE contents. We analyzed a second fragment from the
270 same shell (BP7b), and obtained results that are closer to the rest of studied samples,
271 suggesting that the first sub-sample may have been contaminated by impurities. Alternatively,
272 the range of shell composition could be larger than suggested by the other samples.

273 -Two fragments of the same *Bathymodiolus heckeriae* shell from the West Florida
274 Escarpment were analyzed, with identical results (Fig. 5c). The corresponding patterns are
275 different from those of other methanotrophic mussels. They do not show notable enrichments
276 in light REE like those obtained from the Brine Pool or Bush Hill *Gigantidas*, nor large

277 positive La anomalies like the methanotrophic mussels from China Sea or Melanesia. Their
278 La/La^* (=2.35-2.40) are in the range of seawater values. They are similar to those of
279 thiotrophic mussels (e.g., those from Costa Rican seeps, Fig. 3), with similar negative Ce and
280 positive Y anomalies ($Ce/Ce^*=0.39-0.41$) and positive Y ($Y/Ho=55.2-56.3$).

281 **5/ Discussion**

282 **5.1/ REE characteristics of hydrothermal versus cold seep mussels**

283 Notable differences are apparent between the REE concentrations of mussel shells
284 from hydrothermal vents and those from cold seeps. Bau et al. (2010) showed that mussel
285 shells living in the vicinity of Atlantic hydrothermal vents exhibit characteristic REY patterns,
286 with large positive Eu anomalies [$(Eu/Sm)_{sn}$ up to 5, and >2 in most cases], which are
287 inherited from hydrothermal fluids. The analyses obtained here confirm this observation,
288 showing that all shells from submarine hydrothermal vents display positive Eu anomalies. In
289 contrast, significant positive Eu anomalies are totally absent in shells from cold seeps (Fig. 6),
290 which exhibit $(Eu/Sm)_{sn}$ ratios with little variability (between 1.1 to 1.9). Furthermore,
291 'hydrothermal' shells show much more variable and generally much higher REE
292 concentrations than those from cold seeps, as illustrated by the histograms of Sm
293 concentrations (Fig. 7). Their patterns also sometimes show enrichments in middle REE
294 compared to heavy REE, which can be quantified with $(Tb/Yb)_{sn}$ ratios frequently exceeding
295 2 (Fig. 8). These mid-REE enrichments, combined with presence of significant positive Eu
296 anomalies, reflect the contribution of hydrothermal fluids with REY distributions very
297 different from seawater abundances (Bau and Dulski, 1999; Douville et al., 1999, Schmidt et
298 al., 2007, 2017; Craddock et al. (2010) ; Cole et al., 2014), with no evidence for any presumed
299 biological effect.

300

301 **5.2/ Differences between thiotrophic and methanotrophic mussels at cold seeps**

302 At cold seeps, the REE distributions in mussel shells appear, at least in part, to reflect
303 some characteristics of the surrounding water that they filter (Fig. 8, Fig. 9). Thiotrophic
304 mussels have REE ratios falling in the range of seawater and pore water values. Some
305 samples, however, have slightly higher $(Tb/Sm)_{sn}$ ratios than pore waters, but we do not
306 consider this discrepancy to be very significant since the fluid composition at the sites where
307 our shells originate is not known. As for the mussels from hydrothermal sites, there is no
308 evidence for measurable imprint of any biochemical process involving REE for these animals.

309 The situation is quite different for methanotrophic mussels. While their heavy-REE
310 ratios are similar to those for seawater or pore waters (Fig. 8), light-REE abundances depart
311 substantially from both seawater and pore water values (Fig. 9). They are, in most cases,
312 much more enriched in light-REE than waters, but also more than oil that can be present in
313 some seeps like those of the Gulf of Mexico (Smrzka et al., 2019). As mentioned above,
314 Wang et al (2020) showed that the shells of methanotrophic mussels at methane seeps from
315 the South China Sea display high La anomalies relative to nearby thiotrophic mussel species,
316 clams and seawater. The decoupling of La from other trivalent REE at cold seeps has been
317 interpreted as reflecting the enzymatic activity of associated methanotrophic symbionts, hence
318 indicating aerobic methanotrophy. The new data obtained in this study provide further support
319 to this hypothesis. First, the thiotrophic mussel shells are not particularly enriched in light-
320 REE, and do not show positive La anomalies exceeding usual seawater values, confirming
321 that the enzymatic activity of their symbionts has no notable effect on these elements. On the
322 other hand, the REY patterns obtained for methanotrophic mussel shells are much more
323 variable than those associated with thiotrophic species. Light REE provide a clear-cut
324 separation between most thiotrophic and methanotrophic mussels (Figs. 8 and 9). Except for
325 one sample that will be discussed later, methanotrophic mussels show light-REE enrichments
326 (illustrated by $(Pr/Sm)_{sn}$ or $(Pr/Nd)_{sn}$ ratios, Figs. 8 and 9) commonly accompanied by even
327 more pronounced La enrichments (illustrated by the ratios $(La/Nd)_{sn}$ and La/La^* , Fig. 9). The
328 range of measured light-REE enrichments or La anomalies cannot be explained by local or
329 environmental factors because it far exceeds the range of values known for sediments and
330 marine waters (e.g., Fig. 8 and 9). In agreement with Wang et al. (2020), these enrichments
331 are most likely related to the enzymatic activity of methanotrophic symbionts hosted by the
332 gills of these mussels. It is logical to link them to the degradation of methane to methanol and
333 then to formaldehyde, since REE-dependent (XoxF type) methanol dehydrogenase enzymes
334 are used by these organisms (e.g., Skovran et al., 2011; Semrau et al., 2018; Cotruvo et al.,
335 2019). The large variability of REY patterns obtained for methanotrophic shells suggests that
336 the use of light-REE by these organisms differs from one species to another. For example,
337 some animals generate very large La anomalies in their shells (e.g., *Gigantidas platifrons*
338 from China Sea or *Bathymodiolus* from Edison Seamount), whereas others display only light
339 REE enrichments, with La anomalies similar to those in seawater (e.g., *Gigantidas childressi*
340 from Gulf of Mexico). These differences, which are extremely marked, necessarily reflect
341 different needs in light-REE for the enzymatic activity of these animals. It should be noted,
342 however, that the transfer of these elements from the gills (which are the seat of symbiont

343 activity) to the mantle (which synthesizes the shell) has never been considered until now, and
344 that REE fractionation during this transfer cannot be ignored.

345 One sample, a *Bathymodiolus heckeræ* shell from the West Florida Escarpment (Gulf
346 of Mexico), differs from all other methanotrophic mussel shells analyzed to date (Wang et al.,
347 2020 and this study) in that it lacks significant light REE enrichment, and has an anomaly in
348 La within the range of conventional marine values. This sample even shows REE distributions
349 very similar to those of thiotrophic mussel shells (Fig. 5c). Note that these particular REE
350 signatures associated with *Bathymodiolus heckeræ* cannot be related to analytical artefacts
351 because two separate shell fragments were analyzed, both returning similar results
352 (Supplementary Table 1). Clearly, the symbionts of this mussel did not require light-REE to
353 degrade methane. It is logical to assume that they do not use REE-dependent (XoxF type)
354 methanol dehydrogenase enzymes, but rather Ca-dependent (MxaF type) methanol
355 dehydrogenase enzymes. However, only one shell of this species was available for our study.
356 It would be appropriate at this stage to analyze other samples from this site, and obviously to
357 identify the enzymes used by the mussel symbionts of this species.

358

359 **5.3/ Gd anomalies in mussels from cold seeps**

360 An unexpected result of our study concerns the presence of marked positive Gd
361 anomalies in many cold seep shells (Fig. 10), whereas those from hydrothermal vents show a
362 much narrower range of Gd/Gd* values.

363 Gd anomalies are a common feature of REE sorption in the presence of strong solution
364 complexation, for example with carbonate (dominant in the ocean) or with organic ligands
365 (e.g., Quinn et al., 2006; Christenson and Schijf, 2011). Gd/Gd* ratios on the order of 1.2 are
366 typically encountered in the marine environment. The cold seep mussels investigated here
367 typically display Gd/Gd* ratios exceeding 1.2. We are confident that these anomalies do not
368 correspond to analytical artifacts resulting from biased correction of interferences produced
369 by Ce and Pr oxides. Our procedure effectively corrects for these interferences (e.g., Charles
370 et al., 2021), and the results obtained on standards during the course of the study demonstrate
371 the quality of our analyses (Supplementary Table 1). Moreover, these anomalies were
372 confirmed through multiple measurements of different fragments of the same shells, and
373 cannot possibly relate to inappropriate normalization values, because similar Gd/Gd* values
374 are calculated by normalizing abundances to other shale references or to chondrites (e.g.,

375 Barrat et al., 2012; Bau et al., 2018, not shown). We are also confident that measured Gd
376 excesses in this study were not caused by an artefact related to the calculation of Gd
377 anomalies. Here, Gd anomalies have been calculated by extrapolating Gd* using Tb and Dy
378 concentrations, but similar results are obtained when Gd* is interpolated between Sm and Tb
379 (not shown).

380 Positive Gd anomalies have been measured in mollusk shells living in waters polluted
381 by Gd-based contrast agents (GBCA) used for medical imaging by magnetic resonance (e.g.,
382 Merschel and Bau, 2015; Ponnurangam et al., 2016; Akagi and Edanami, 2017; Le Goff et al.,
383 2019). Even if this pollution is now common in coastal waters worldwide, it is highly unlikely
384 that anthropogenic Gd pollution affects the deep sea at which our samples were collected. We
385 tentatively propose that these Gd anomalies are the result of either biological fractionation or
386 that they reflect the composition of the water filtered by the mussels. Since Gd anomalies are
387 present in the shells of both thiotrophic and methanotrophic animals, they are probably not the
388 result of any specific enzymatic activity related to nutritional symbiosis. It is possible that
389 cold seep mussels fractionate Gd for an undiscovered use in other biological functions. One
390 may wonder why these anomalies are not ubiquitous features of bivalve shells, including in
391 thiotrophic species encountered at hydrothermal vents, where mussel shells lack the marked
392 Gd anomalies. As an alternative, Gd anomalies could be inherited from water filtered by
393 mussels. Recently, Möller et al. (2021) reported high Gd/Gd* ratios in natural,
394 uncontaminated, spring waters and hypersaline waters (e.g., Dead Sea). Gd/Gd* ratios close
395 to 1.7 or higher are unknown in seawaters and oceanic hydrothermal fluids. What about
396 methane-rich fluids from cold seeps? There are limited REE data for methane-rich fluids at
397 cold seeps (e.g., Himmler et al., 2013; Lemaitre et al., 2014). However, some of their
398 characteristics can be inferred from the composition of the carbonates they deposit (e.g.,
399 Smrzrka et al., 2020; Bayon et al., 2020a). To date, it has not been convincingly shown that
400 cold seeps carbonates can exhibit such anomalies, making it more than hypothetical that they
401 are present in cold seeps fluids. The origin and significance of the Gd anomalies observed in
402 cold seeps mussel shells is not yet understood.

403

404 **6/ Conclusions and perspectives**

405 In this study, we compared REE abundances in deep-water mussel shells from various
406 hydrothermal and cold seep systems worldwide, confirming that animals living at

407 hydrothermal sites display compositional shell characteristics of surrounding fluids such as
408 positive Eu anomalies (Bau et al., 2010). The REE distribution in bivalve shells at submarine
409 methane seeps provides a window into the enzymatic activity of associated symbionts. Unlike
410 thiotrophic mussels, methanotrophic species whose symbionts use light-REE to degrade
411 methane, show characteristic light-REE enrichments in their shells. Our results confirm that
412 only methanotrophic mussels display distinctive positive La anomalies, but selective La
413 enrichments are not systematic to all species analyzed. The degree of light REE enrichment in
414 shells probably depends on the distribution pattern of hosted symbionts and associated
415 enzymatic activities, suggesting regional variability. For instance, only shells from western
416 Pacific sites displayed strong positive La anomalies in this study. At this stage, it is unclear
417 whether this characteristic relates to the presence of specific symbiont lineages. Future
418 investigations of other mussel species from additional sites combined with symbiont
419 characterization will be required to address this issue. In future studies, REE concentrations in
420 abyssal mussel shells could be used to distinguish methanotrophic from thiotrophic species,
421 hence serving as tools for identifying their general enzymatic pathway. This novel approach
422 could be also applied to the sedimentary record and the investigation of fossil shells in ancient
423 seep deposits, providing of course that diagenesis or any other post-depositional processes
424 have not modified their REE abundances. Overall, these findings open up important
425 multidisciplinary perspectives in biology, Earth and environmental sciences, requiring further
426 improvements in our understanding of the REE biogeochemistry and inventory in organisms,
427 and their role in enzymatic activities and metabolic pathways. Additional work will be also
428 needed to assess the impact of life on REE cycling in the ocean, something that has been
429 largely overlooked until now. Our new data reinforce the idea that methanotrophic organisms,
430 at least those using REE-based enzymes, can leave a distinctive chemical fingerprint in rocks,
431 in particular in methane-derived carbonates at cold seeps. Some of these authigenic
432 carbonates contain organic-rich aragonitic cements exhibiting high light-REE enrichments
433 (Zwicker et al., 2018). So far, these cements have been interpreted as fossil biofilms
434 (Hagemann et al., 2013), but it is very tempting to see here the imprint of aerobic
435 methanotrophic activity. Finally, we draw the attention of the large geochemical community
436 studying ancient marine sedimentary formations of Precambrian age, to the interest of
437 carrying out detailed investigations coupling REE to other conventional biogeochemical
438 proxies such as stable isotopes in order to detect the emergence of aerobic methanotrophy on
439 Earth.

440

441

442 *Acknowledgements.*

443 This project was founded by “Laboratoire d’Excellence” LabexMER (ANR-10-LABX-19)
444 and co-funded by grants from the French Government. Shell fragments from museum
445 specimens at SIO-BIC were provided by Charlotte Seid and Greg Rouse. Specimens from
446 Costa Rica were collected under permits SINAC-CUS-PI-R-035-2017 and SINAC-CUSBSE-
447 PI-R-032-2018, issued by the Ministerio de Ambiente y Energía (MINAE), Sistema Nacional
448 de Areas de Conservación (SINAC). Collection of the Costa Rica specimens was funded by
449 the United States National Science Foundation, grant # OCE-1634172 to Greg Rouse and Lisa
450 Levin. We thank the captain and crew of the R/V *Atlantis*, the pilots and technicians of the
451 HOV *Alvin*, chief scientist Erik Cordes, and the scientists of cruises AT37-13 and AT42-03
452 for assistance with specimen collection in Costa Rica. *Gigantidas childressi* samples were
453 collected by R.S. Carney and made available through grant GM-09-01-08 from the US Bureau
454 of Ocean Energy Management to R.S. Carney and B. Fry of Louisiana State University. We
455 thank Balz Kamber for the editorial handling, Johan Schijf and Dong Feng for their
456 constructive reviews.

457

458 **References**

459

460 Akagi T., Edanami K. (2017) Sources of rare earth elements in shells and soft tissues of bivalves from Tokyo
461 Bay. *Marine Chemistry* **194**, 55–62.

462 Barrat J.A., Keller F., Amossé J., Taylor R.N., Nesbitt R.W., Hirata T. (1996) Determination of rare earth
463 elements in sixteen silicate reference samples by ICP-MS after Tm addition and ion exchange separation.
464 *Geostandards Newsletter* **20**, 1, 133-140.

465 Barrat J.A., Zanda B., Moynier F., Bollinger C., Liorzou C., and Bayon G. (2012) Geochemistry of CI
466 chondrites: Major and trace elements, and Cu and Zn isotopes. *Geochim. Cosmochim. Acta* **83**, 79-92.

467 Barrat J.A., Dauphas N., Gillet P., Bollinger C., Etoubleau J., Bischoff A., Yamaguchi A. (2016) Evidence from
468 Tm anomalies for non-CI refractory lithophile element proportions in terrestrial planets and achondrites.
469 *Geochim. Cosmochim. Acta*, **176**, 1-17.

470

471 Barrat J.A., Bayon G., Wang X., Le Goff S., Rouget M.L., Gueguen B., Ben Salem B. (2020) A new chemical
472 separation procedure for the determination of rare earth elements and yttrium abundances in carbonates by
473 ICP-MS. *Talanta* **219**, 121244.

474

475 Bau M. and Dulski P. (1999) Comparing yttrium and rare earths in hydrothermal fluids from the Mid-Atlantic
476 Ridge: implications for Y and REE behaviour during near-vent mixing and for the Y/Ho ratio of
477 Proterozoic seawater. *Chem. Geol.* **155**, 77-90.

478

479 Bau M., Balan S., Schmidt K., Koschinsky, A. (2010) Rare earth elements in mussel shells of the *Mytilidae*
480 family as tracers for hidden and fossil high-temperature hydrothermal systems. *Earth Planet Sci. Lett.* **299**,
481 310-316.

482

483 Bau M., Schmidt K., Koschinsky A., Hein J.R., Kuhn T., Usui A. (2014) Discriminating between different
484 genetic types of marine ferro-manganese crusts and nodules based on rare earth elements and yttrium,
485 *Chem. Geol.* **381**, 1-9.

486

487 Bau M., Schmidt K., Pack A., Bendel B., Kraemer D. (2018) The European Shale: an improved data set for
488 normalization of rare earth elements and yttrium concentrations in environmental and biological samples
489 from Europe. *Applied Geochem.* **90**, 142-149.
490

491 Bayon G., Lemaitre N., Barrat J.A., Wang X., Feng D., Duperron S. (2020a) Microbial utilization of rare earth
492 elements at cold seeps related to aerobic methane oxidation. *Chem. Geol.* **555**, 119832.
493

494 Bayon G., Lambert T., Vigier N., De Dekker P., Freslon N., Jang K., Larkin C.S., Piotrovski A.M., Tachikawa
495 K., Thollon M., Tipper E.D. (2020b) Rare earth element and neodymium isotope tracing of sedimentary
496 rock weathering. *Chem. Geol.* **553**, 119794.
497

498 Brzechffa C., Goffredi S.K. (2021) Contrasting influences on bacterial symbiont specificity by co-occurring
499 deep-sea mussels and tubeworms. *Environmental Microbiology Reports* **13**, 104-111.
500

501 Cavanaugh, C. M., Gardiner, S. L., Jones, M. L., Jannasch, H. W., Waterbury, J. B. (1981) Prokaryotic cells in
502 the hydrothermal vent tube worm *Riftia pachyptila* Jones: possible chemoautotrophic symbionts. *Science*
503 **213**, 340-342.
504

505 Cavanaugh, C. M., Levering, P. R., Maki, J. S., Mitchell, R., Lidstrom, M. E. (1987) Symbiosis of
506 methylotrophic bacteria and deep-sea mussels. *Nature* **325**, 346-348.
507

508 Chanton JP, Martens CS, Paull CK, Coston JA (1993) Sulfur isotope and porewater geochemistry of Florida
509 Escarpment seep sediments. *Geochim. Cosmochim. Acta* **57**, 1253-1266
510

511 Charles C., Barrat J.A., Pelleter E. (2021) Trace element determinations in Fe-Mn oxides by high resolution
512 ICP-MS after Tm addition. *Talanta* **233**, 122446.
513

514 Childress, J. J. et al. (1986) A methanotrophic marine molluscan (*Bivalvia*, *Mytilidae*) symbiosis: mussels fueled
515 by gas. *Science* **233**, 1306-1308.
516

517 Christenson E.A. and Schijf J. (2011) Stability of YREE complexes with the trihydroxamate siderophore
518 desferrioxamine B at seawater ionic strength. *Geochim. Cosmochim. Acta* **75**, 7047-7062.
519

519 Cole C.S., James R.H., Connelly D.P. and Hathorne E.C. (2014) Rare earth elements as indicators of
520 hydrothermal processes within the East Scotia subduction zone system. *Geochim. Cosmochim. Acta* **140**,
521 20-38.
522

523 Corliss J.B. and Ballard R.D. (1977) Oases of life in the cold abyss. *Natl. Geograph.* **152**, 441-453.
524

525 Cotruvo, jr., J.A. (2019) The chemistry of lanthanides in biology: recent discoveries, emerging principles, and
526 technological applications. *ACS Central Science* **5**, 1496-1506.
527

528 Craddock P.R., Bach W., Seewald J.S., Rouxel O.J., Reeves E. and Tivey M.K. (2010) Rare earth element
529 abundances in hydrothermal fluids from the Manus Basin, Papua New Guinea: indicators of sub-seafloor
530 hydrothermal processes in back-arc basins. *Geochim. Cosmochim. Acta* **74**, 5494-5513.
531

532 Douville, E., Bienvenu, P., Charlou, J.L., Donval, J.P., Fouquet, Y., Appriou, P., Gamo, T. (1999) Yttrium and
533 the rare earth elements in fluids from various deep-sea hydrothermal systems. *Geochim. Cosmochim. Acta*
534 **63**, 627-643.
535

536 Duperron, S., Sibuet, M., MacGregor, B.J., Kuypers, M.M.M., Fisher, C.R., Dubilier, N. (2007) Diversity,
537 relative abundance and metabolic potential of bacterial endosymbionts in three *Bathymodiulus* mussel
538 species from cold seeps in the Gulf of Mexico. *Environmental Microbiology* **9**, 1423-1438.
539

540 Elderfield H. (1988) The oceanic chemistry of the rare-earth elements. *Philosophical Transaction of the Royal*
541 *Society of London. Series A, Mathematical and Physical Sciences* **325**, 105-126.
542

543 Felbeck, H. (1981) Chemoautotrophic potential of the hydrothermal vent tube worm, *Riftia pachyptila* Jones
544 (*Vestimentifera*). *Science* **213**, 336-338.
545

- 546 Feng D., Peckmann J., Li N., Kiel S., Qiu J.W., Liang Q., Carney R.S., Peng Y, Tao J., Chen D. (2018) The
547 stable isotope fingerprint of chemosymbiosis in the shell organic matrix of seep-dwelling bivalves.
548 *Chem. Geol.* **479**, 241-250
549
- 550 Hagemann A., Leefman T., Peckmann J., Hoffmann V.E., Thiel, V. (2013) Biomarkers from individual
551 carbonate phases of an Oligocene cold-seep deposit, Washington State, USA. *Lethaia* **46**, 7-18.
552
- 553 Henderson, P. (1984) General geochemical properties and abundances of the rare earth elements, in: P.
554 Henderson (Ed.), *Rare Earth Element Geochemistry*, Elsevier, 1984, pp. 1–32.
555
- 556 Herzig P.M., Hanningen M.D., Stoffers P. and the shipboard scientific party (1998) Petrology, gold
557 mineralisation and biological communities at shallow submarine volcanoes of the New Ireland fore-arc
558 (Papua-New Guinea): preliminary results of R/V Sonne cruise SO-133. *Inter-Ridge News* **7**, 34-38.
- 559 Himmler, T., Haley B., Torres M.E., Klinkhammer G.P., Bohrmann G., Peckmann J. (2013) Rare earth element
560 geochemistry in cold-seep pore waters of Hydrate Ridge, northeast Pacific Ocean. *Geo-Mar. Lett.* **33**, 369–
561 379.
562
- 563 Kenk V.C. & Wilson B.R. (1985). A new mussel (*Bivalvia*, *Mytilidae*) from hydrothermal vents, in the
564 Galapagos Rift zone. *Malacologia* **26**, 253-271.
565
- 566 Le Goff S., Barrat J.A., Chauvaud L., Paulet Y.M., Gueguen B., Ben Salem D. (2019) Compound-specific
567 recording of gadolinium pollution in coastal waters by great scallops. *Scientific Reports* **9**, 8015.
568
- 569 Lemaitre N., Bayon G., Ondréas H., Caprais J.C., Freslon N., Bollinger C., Rouget M.L., de Prunelé A., Ruffine
570 L., Olu-Le Roy K., Sarthou G. (2014) Trace element behaviour at cold seeps and the potential export of
571 dissolved iron to ocean. *Earth Planet. Sci. Lett.* **404**, 376-388.
572
- 573 Levin, L.A., Orphan, V.J., Rouse, G.W., Rathburn, A.E., Ussler, W., Cook, G.S., Goffredi, S. K., Perez, E.M.,
574 Warren, A., Grupe, B.M., Chadwick, G., Strickrott, B. (2012) A hydrothermal seep on the Costa Rica
575 margin: middle ground in a continuum of reducing ecosystems. *Proc. R. Soc. B Biol. Sci.* **279**, 2580–2588.
- 576 Levin, L.A., Mendoza, G.F., Grupe, B.M., Gonzalez, J.P., Jellison, B., Rouse, G., Thurber, A.R., Warren, A.
577 (2015) Biodiversity on the rocks: macrofauna inhabiting authigenic carbonate at Costa Rica methane seeps.
578 *PloS One* **10**, e0131080.
- 579 Macavoy S.E., Carney R.S., Morgan E., Macko S.A. (2008) Stable isotope variation among the mussel
580 *Bathymodiolus childressi* and associated heterotrophic fauna at four cold-seep communities in the Gulf of
581 Mexico. *J. Shellfish Res.* **27**, 147-151.
582
- 583 Martens C.S., Chanton J.P., Paull C.K. (1991) Biogenic methane in the Florida Escarpment brine seeps. *Geology*
584 **19**, 851–857.
585
- 586 McCowin M.F., Feehery C., Rouse G.W. (2020) Spanning the depths or depth-restricted: three new species of
587 *Bathymodiolus* (*Bivalvia*, *Mytilidae*) and a new record for the hydrothermal vent *Bathymodiolus*
588 thermophiles at methane seeps along the Costa Rica margin. *Deep-Sea Res. 1* **164**, 103322.
- 589 Merschel G., Bau M. (2015) Rare earth elements in the aragonitic shell of freshwater mussel *Corbicula fluminea*
590 and the bioavailability of anthropogenic lanthanum, samarium and gadolinium in river water. *Sci. Total*
591 *Environment* **533**, 91-101.
592
- 593 Meyer A.C.S., Grundle D., Cullen J.T. (2021) Selective uptake of rare earth elements in marine systems as an
594 indicator of and control on aerobic bacterial methanotrophy. *Earth Planet. Sci. Lett.* **558**, 116756.
595
- 596 Möller P, Dulski P., De Lucia M. (2021) REY patterns and their natural anomalies in waters and brines: the
597 correlation of Gd and Y anomalies. *Hydrology* **8**, 116, <https://doi.org/10.3390/hydrology8030116>.
598
- 599 Northdurft L.D., Webb G.E., Kamber B.S. (2004) Rare earth element geochemistry of Late Devonian reefal
600 carbonates, Canning Basin, Western Australia: confirmation of a seawater REE proxy in ancient limestones
601 *Geochim. Cosmochim. Acta* **68**, 263-283.

602 Ozaki T., Enomoto S., Minai Y., Ambe S., Ambe F., Tominaga T. (1997) Determination of Lanthanides and
603 other trace elements in ferns by instrumental neutron activation analysis. *J. Radioanalytical Nuclear Chem.*
604 **217**, 117-124.

605 Paull C.K., Hecker B., Commeau R., Freeman-Lynde R.P., Neumann C., Corso W.P., Golubic S., Hook J.E.,
606 Sikes E., Curray J. (1984) Biological communities at the Florida Escarpment resemble hydrothermal vent
607 taxa. *Science* **226**, 965-967.

608
609 Paull C.K., Jull A.J.T., Toolin L.J., Linick T. (1985) Stable isotope evidence for chemosynthesis in an abyssal
610 seep community. *Nature* **317**, 709-711.

611
612 Paull, C.K., Martena, C.S., Chanton, J.P., Neumann, A.C., Coston, J., Jull, A.J.T., Toolin, L.J. (1989) Old carbon
613 in living organisms and young CaCO₃ cements from abyssal brine seeps. *Nature* **342**, 166-168.

614 Petersen J.M., Zielinski F.U., Pape T., Seifert R., Moraru C., Amann R., Hourdez S., Girguis P.R., Wankel
615 S.D., Barbe V., Pelletier E., Fink D., Borowski C., Bach W., Dubilier N. (2011) Hydrogen is an energy
616 source for hydrothermal vent symbioses. *Nature* **476**, 176-180.

617 Pol, A., Barends T.R.M., Dietl A., Khadem A.F., Eygensteyn J., Jetten M.S.M., Op Den Camp H.J.M. (2014)
618 Rare earth metals are essential for methanotrophic life in volcanic mud pots. *Environmental Microbiology*
619 **16**, 255-264.

620 Ponnurangam, A., Bau, M., Brenner, M., Kochinsky, A. (2016) Mussel shells of *Mytilus edulis* as bioarchives of
621 the distribution of rare earth elements and yttrium in seawater and the potential impact of pH and
622 temperature on their partitioning behavior. *Biogeosciences* **13**, 751-760.

623 Pourmand, A., Dauphas, N., Ireland, T.J. (2012) A novel extraction chromatography and MC-ICP-MS technique
624 for rapid analysis of REE, Sc and Y: Revising CI-chondrite and Post-Archean Australian Shale (PAAS)
625 abundances. *Chem. Geol.* **291**, 38-54.

626
627 Quinn K.A., Byrne R.H., Schijf J. (2006) Sorption of yttrium and rare earth elements by amorphous ferric
628 hydroxide: Influence of solution complexation with carbonate. *Geochim. Cosmochim. Acta* **70**, 4151-4165.

629
630 Ramachandran, A. & Walsh, D. A. (2015) Investigation of XoxF methanol dehydrogenases reveals new
631 methylotrophic bacteria in pelagic marine and freshwater ecosystems. *FEMS Microbiology Ecology* **91**(10),
632 fiv105.

633
634 Riekenberg P.M., Carney R.S., Fry, B. (2018) Shell carbon isotope indicators of metabolic activity in the deep-
635 sea mussel *Bathymodiolus childressi*. *Deep Sea res. Part. 1* **134**, 48-54.

636
637 Sahling, H., Masson, D.G., Ranero, C.R., Hühnerbach, V., Weinrebe, W., Klauke, I., Bürk, D., Brückmann, W.,
638 Suess, E. (2008) Fluid seepage at the continental margin offshore Costa Rica and southern Nicaragua.
639 *Geochem. Geophys. Geosyst.* **9**, Q05S05.

640
641 Schmidt K., Koschinsky A., Garbe-Schönberg D., Decarvalho L. and Seifert R. (2007) Geochemistry of
642 hydrothermal fluids from the ultramafic-hosted Logatchev hydrothermal field, 15°N on the Mid-Atlantic
643 Ridge: temporal and spatial investigation. *Chem. Geol.* **242**, 1-21.

644
645 Schmidt K., Garbe-Schönberg D., Hannington M.D., Anderson M.O., Bühring B., Haase K., Haruel C., Lupton
646 J., Koschinsky A. (2017) Boiling vapour-type fluids from the Nifonea vent field (New Hebrides Back-Arc,
647 Vanuatu, SW Pacific): geochemistry of an early-stage, post-eruptive hydrothermal system. *Geochim.*
648 *Cosmochim. Acta* **207**, 185-209.

649
650 Semrau, J.D., Dispirito, A.A., GU, W., Yoon, S. (2018) Metals and Methanotrophy. *Applied and Environmental*
651 *Microbiology* **84**, e02289-17.

652
653 Shiller, A.M., Chan, E.W., Joung D.J., Redmond, M.C., Kessler, J.D. (2017) Light rare earth element depletion
654 during *Deepwater Horizon* blowout methanotrophy. *Scientific Reports* **7**, 10389, DOI:10.1038/s41598-017-
655 11060-z

656

657 Skovran, E., Palmer, A. D., Rountree, A. M., Good, N. M., Lidstrom, M. E. (2011) XoxF is required for
658 expression of methanol dehydrogenase in *Methylobacterium extorquens* AM1. *J. Bacteriol.* 193, 6032-
659 6038.

660

661 Smrzka D., Zwicker J., Misch D., Walkner C., Gier S., Monien P., Bohrmann G., Peckmann J. (2019) Oil
662 seepage and carbonate formation: A case study from the southern Gulf of Mexico. *Sedimentology* **66**, 2318-
663 2353.

664

665 Smrzka D., Feng D., Himmler T., Zwicker J., Hu Y., Monien P., Tribovillard N., Chen D., Peckmann J. (2020)
666 Trace elements in methane-seep carbonates: potentials, limitations, and perspectives. *Earth Sci Rev.***208**,
667 103263.

668

669 Taubert M. *et al.* (2015) XoxF encoding an alternative methanol dehydrogenase is widespread in coastal marine
670 environments. *Environ. Microbiol.* 17, 3937–3948.

671

672 Tommasi F., Thomas P.J., Pagano G., Perono G.A., Oral R., Lyons D.M., Toscanesi M., Trifuoggi M. (2021)
673 Review of rare earth elements as fertilizers and feed additives: a knowledge gap analysis. *Archives of*
674 *Environmental Contamination and Toxicology* **81**, 531-540.

675

676 von Cosei R., Janssen R. (2008) Bathymodioline mussels of the *Bathymodiolus* (s.l.) *childressi* clade from
677 methane seeps near Edison Seamount, New Ireland, Papua New Guinea. *Arch. Molluskenkunde* **137**, 195-
678 224.

679

680 Wang X., Barrat J.A., Bayon G., Chauvaud L., Feng D. (2020) Lanthanum anomalies as fingerprints of
681 methanotrophy. *Geochem. Persp. Let.* **14**, 26–30.

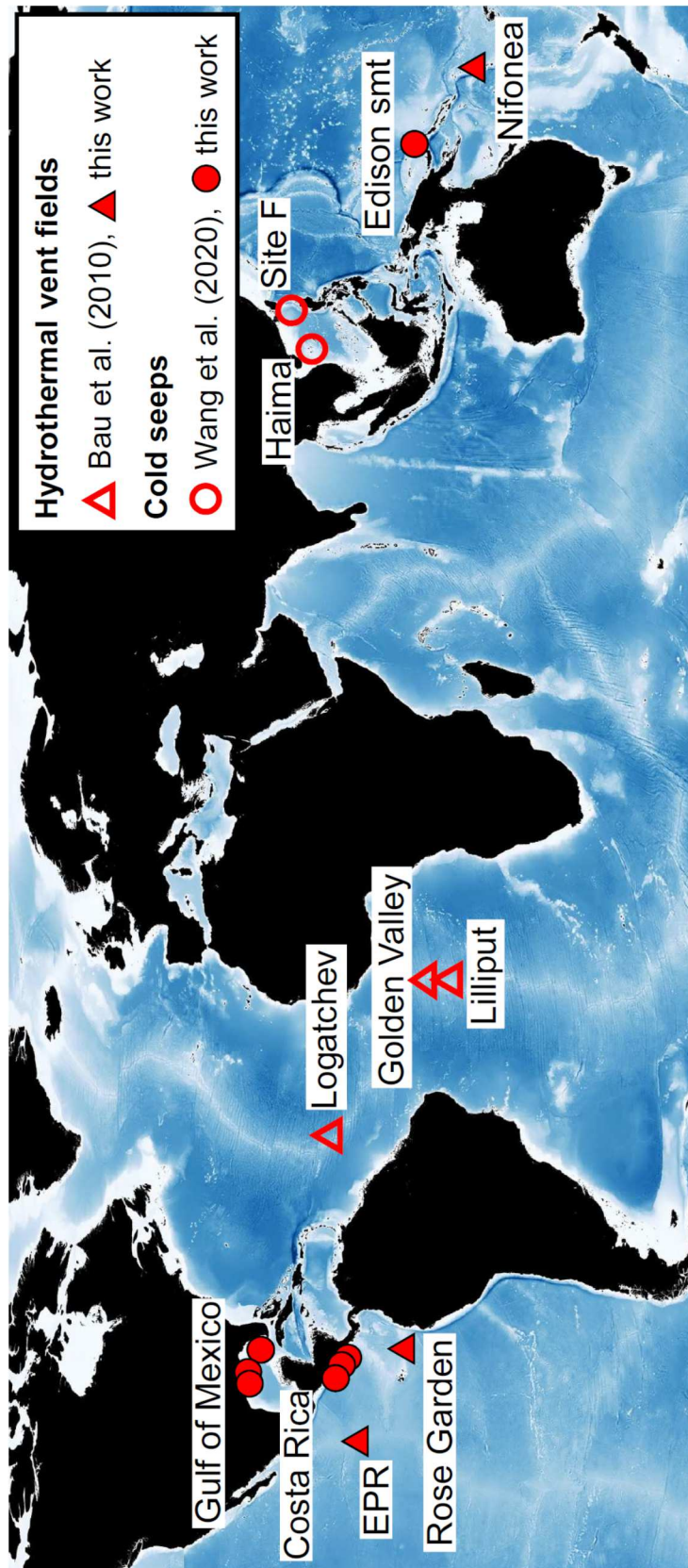
682

683 Xu T, Feng D., Tao J., Qiu J-W. (2019) A new species of deep-sea mussel (Bivalvia: Mytilidae; Gigantidas)
684 from the South China Sea: Morphology, phylogenetic position, and gill-associated microbes. *Deep Sea*
685 *Res.*, Pt. 1 **146**, 79-90.

686

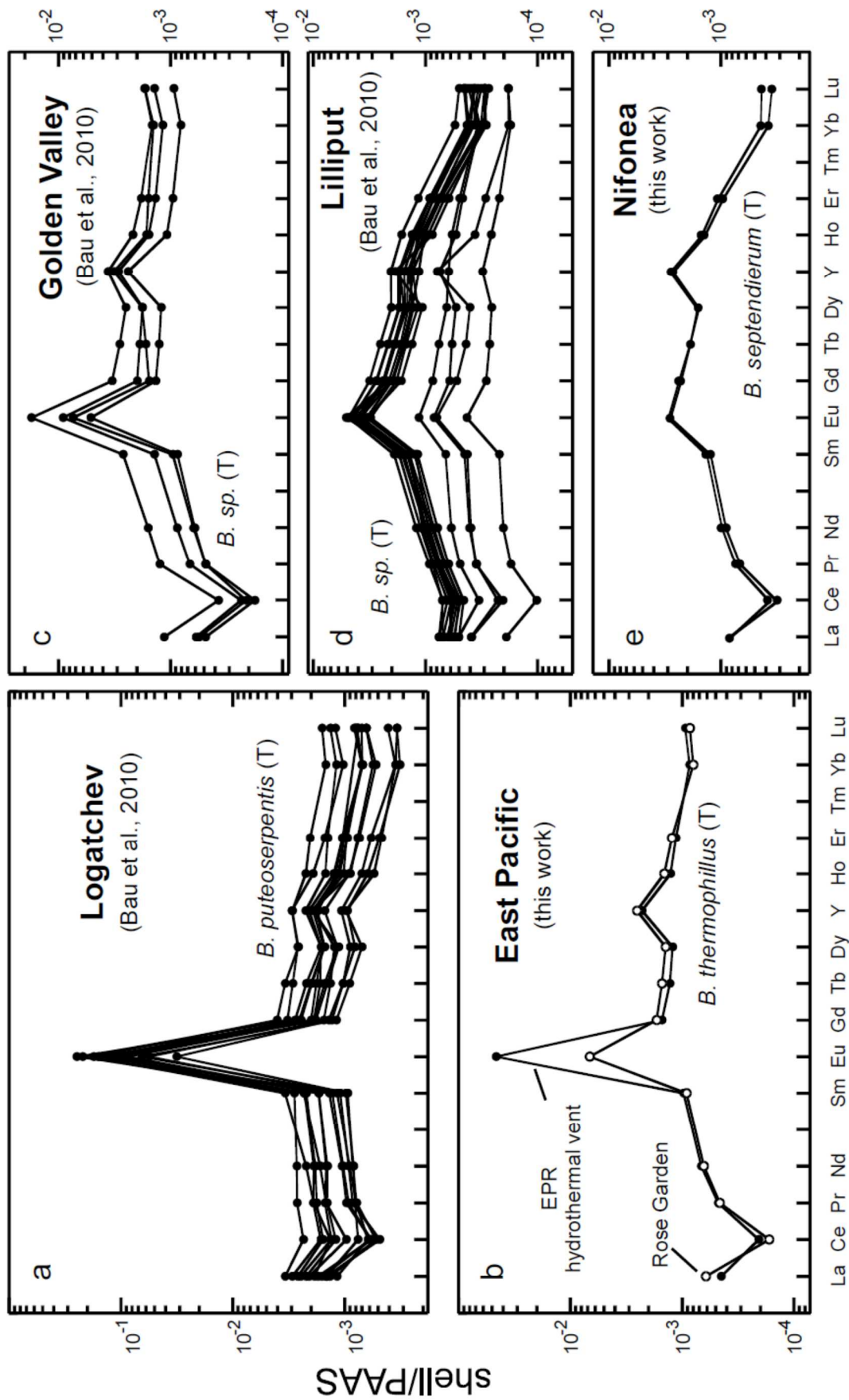
687 Zwicker J., Smrzka D., Himmler T., Monien P., Gier S., Goedert J.L., Peckmann J. (2018) Rare earth elements
688 as tracers for microbial activity and early diagenesis: A new perspective from carbonate cements of ancient
689 methane-seep deposits. *Chem. Geol.* **501**, 77-85.

690



691
 692
 693
 694
 695
 696

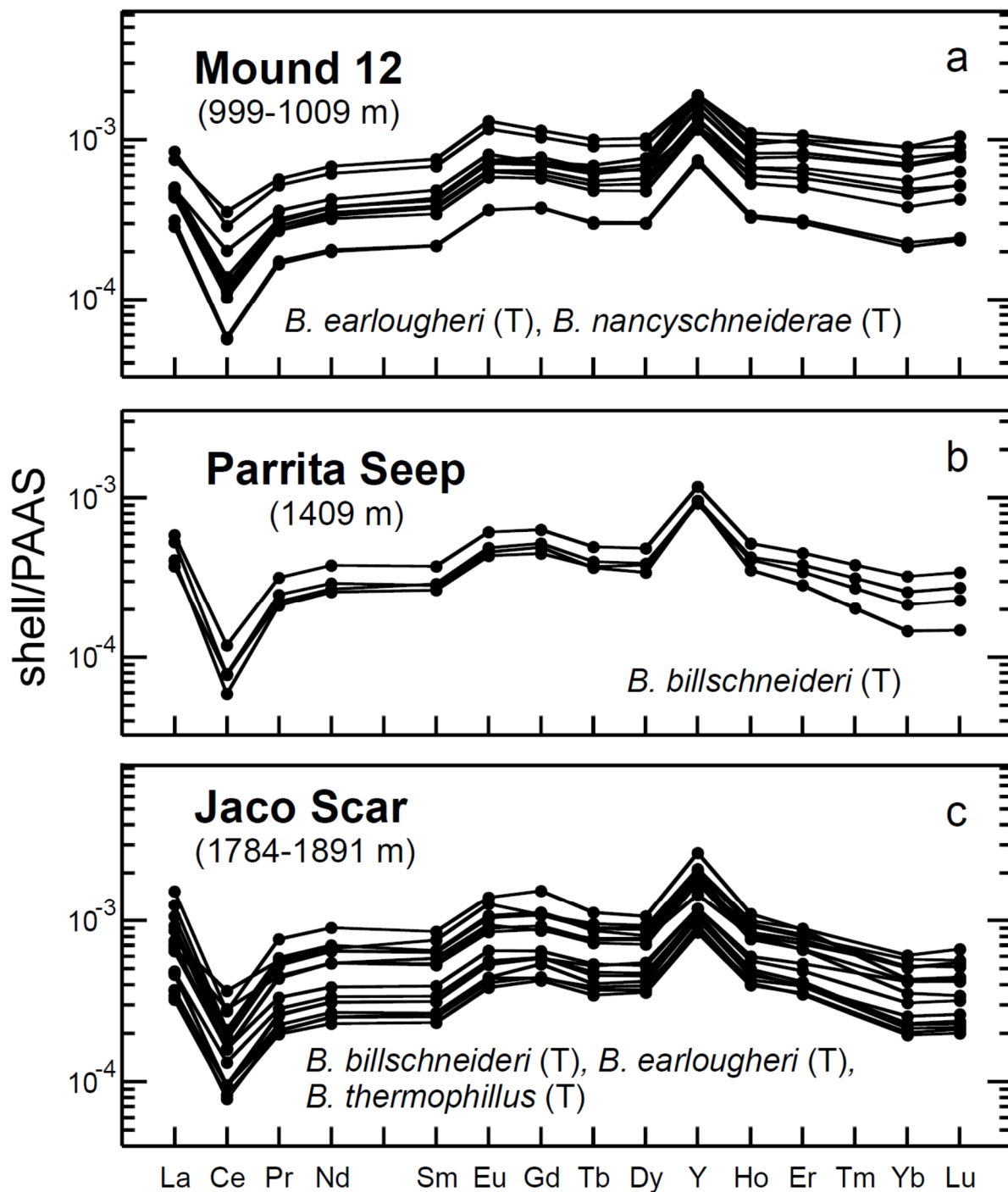
Figure 1. World map and location of the hydrothermal vents and cold seeps where mussels have been analyzed for REE and Y abundances (Bau et al., 2010; Wang et al., 2020; this study).



697
698
699

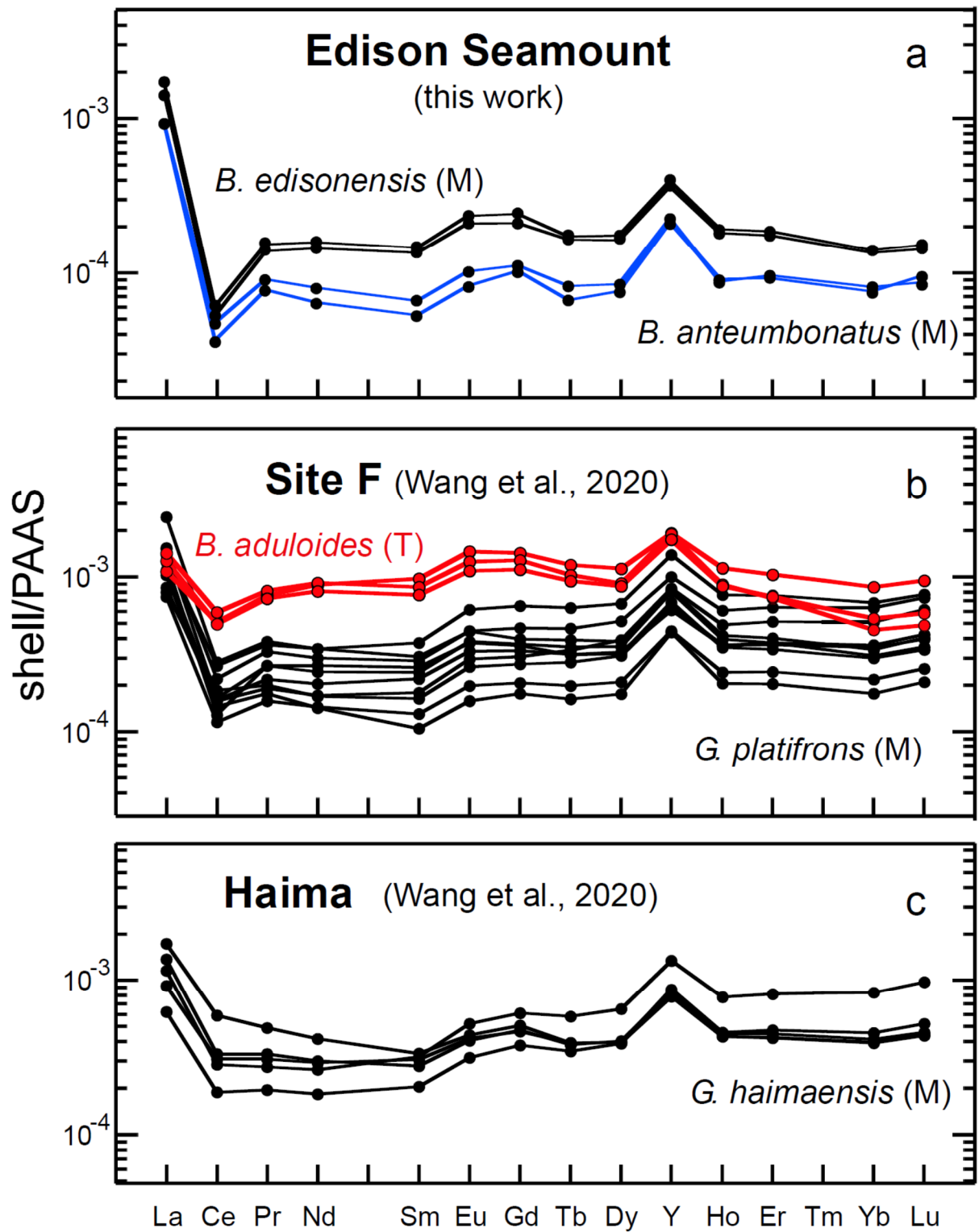
Figure 2. PAAS-normalized REY patterns for shells of thiotrophic (T) mussels from hydrothermal vents.

700
701
702
703
704
705



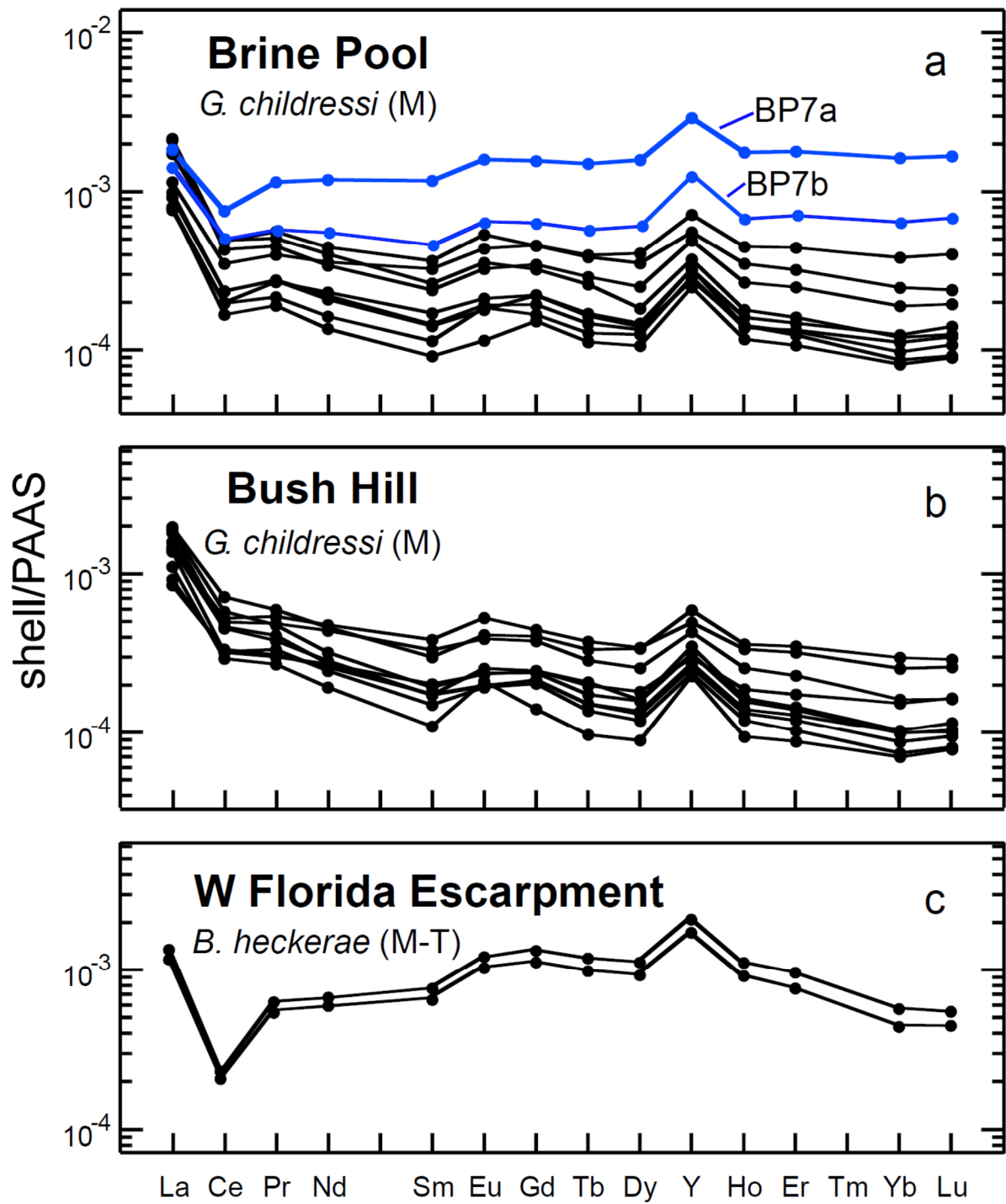
706
707
708
709
710
711
712

Figure 3. PAAS-normalized REY patterns for mussel shells from vents located west of Costa Rica. Here, all the mussels are thiotrophic (T).



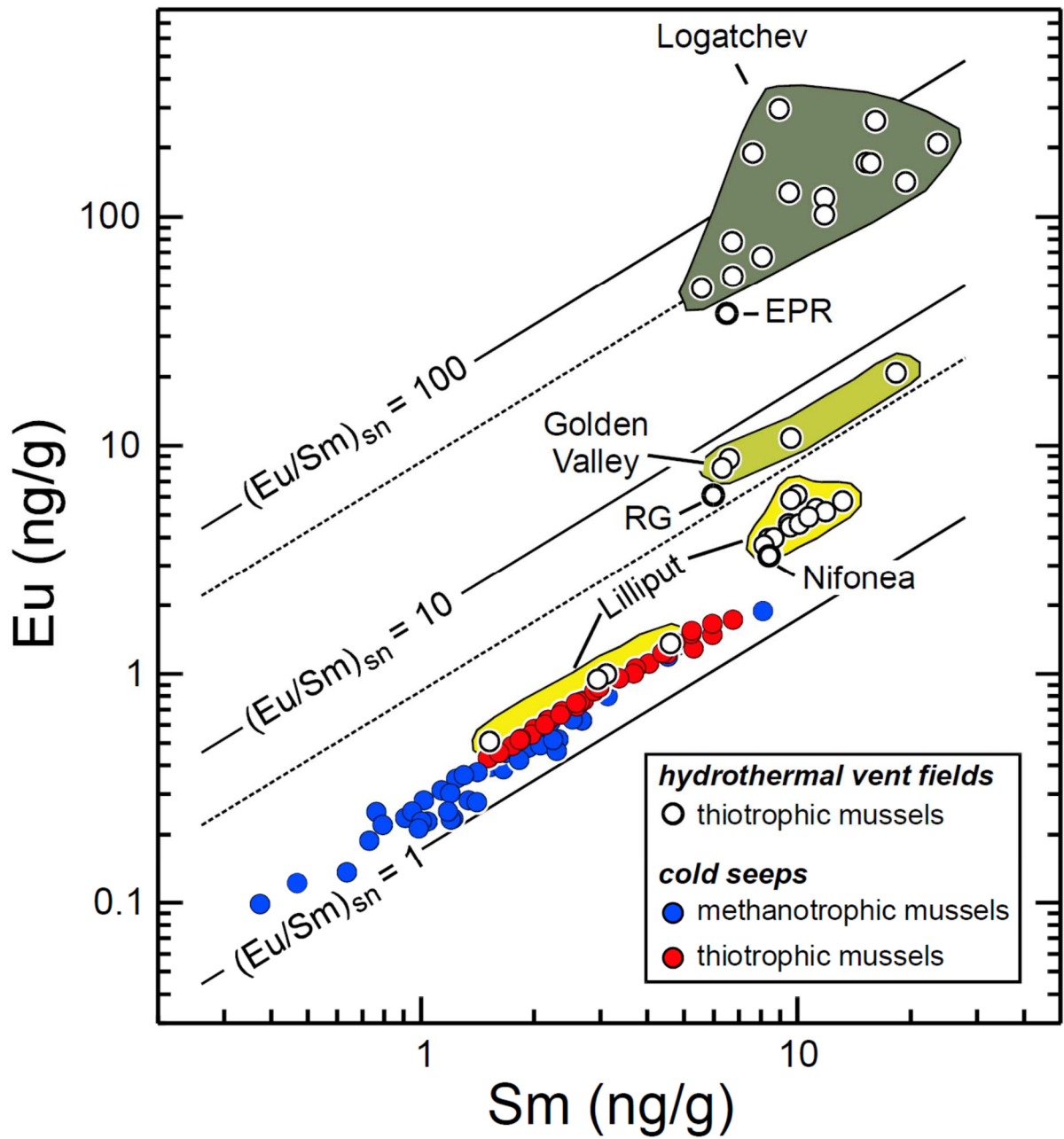
713
714
715
716
717
718
719
720
721
722

Figure 4. PAAS-normalized REY patterns for mussel shells from cold seeps located in the China Sea (site F and Haima, Wang et al., 2020), and from Edison Seamount (this work). *Bathymodiolus aduloides* mussels are thiotrophic (T). The others are methanotrophic (M).



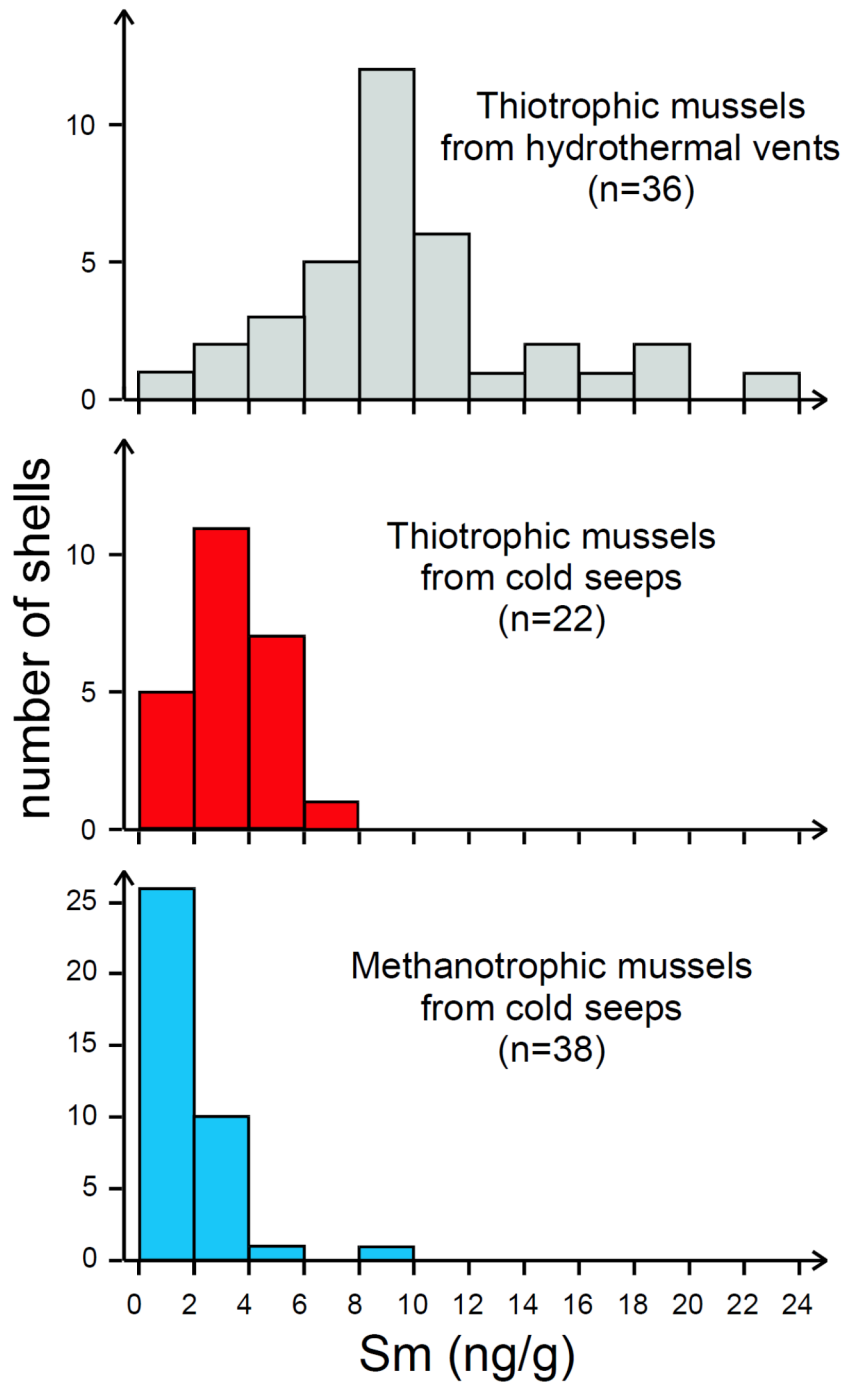
723
724
725
726
727
728
729

Figure 5. PAAS-normalized REY patterns for mussel shells from the Gulf of Mexico (M: methanotrophic; T: thiotrophic).



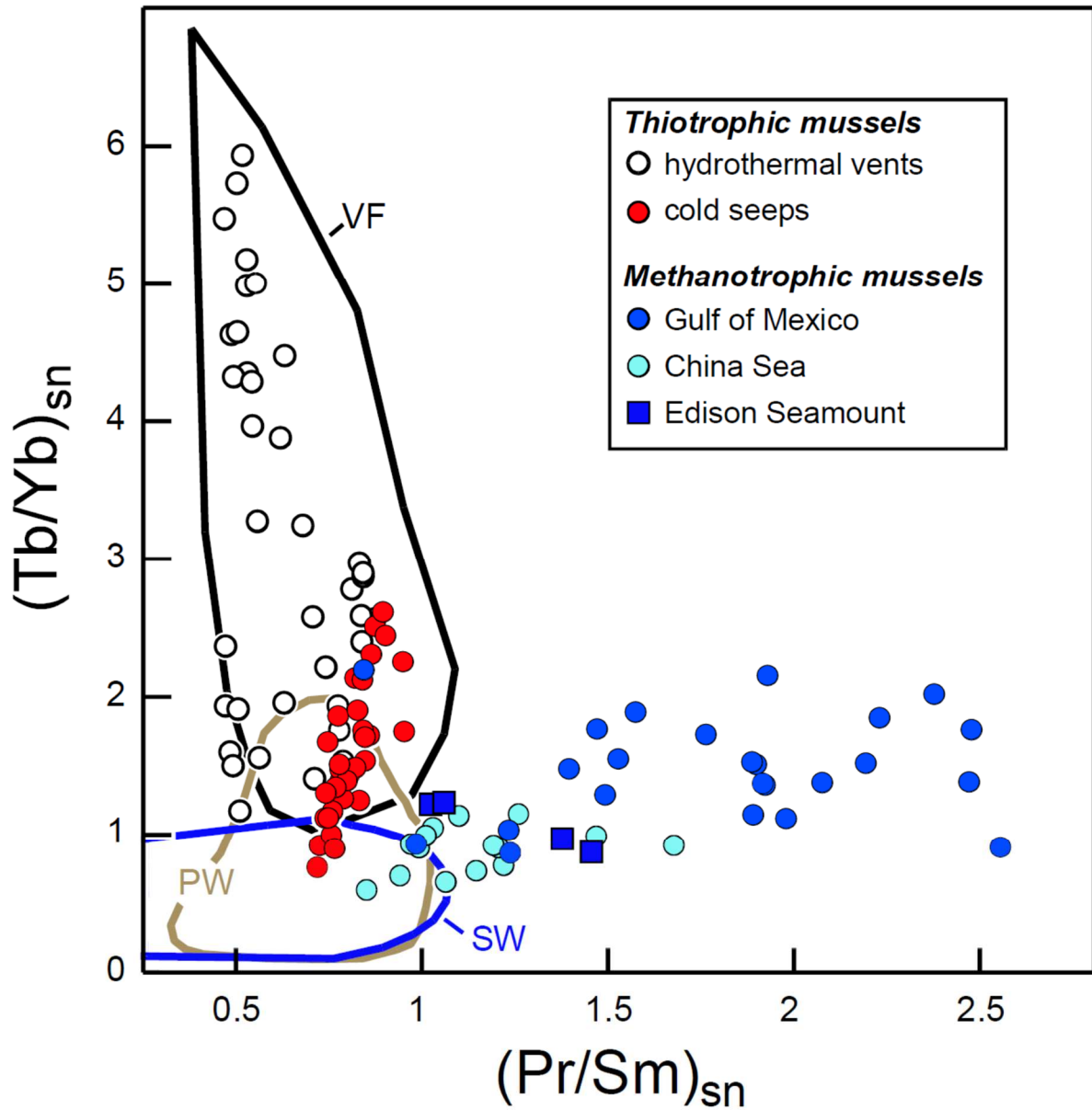
730
 731
 732
 733
 734
 735
 736
 737

Figure 6. Eu vs. Sm plot for mussel shells from hydrothermal vents and cold seeps (data from Bau et al., 2010, Wang et al., 2020, and this study).



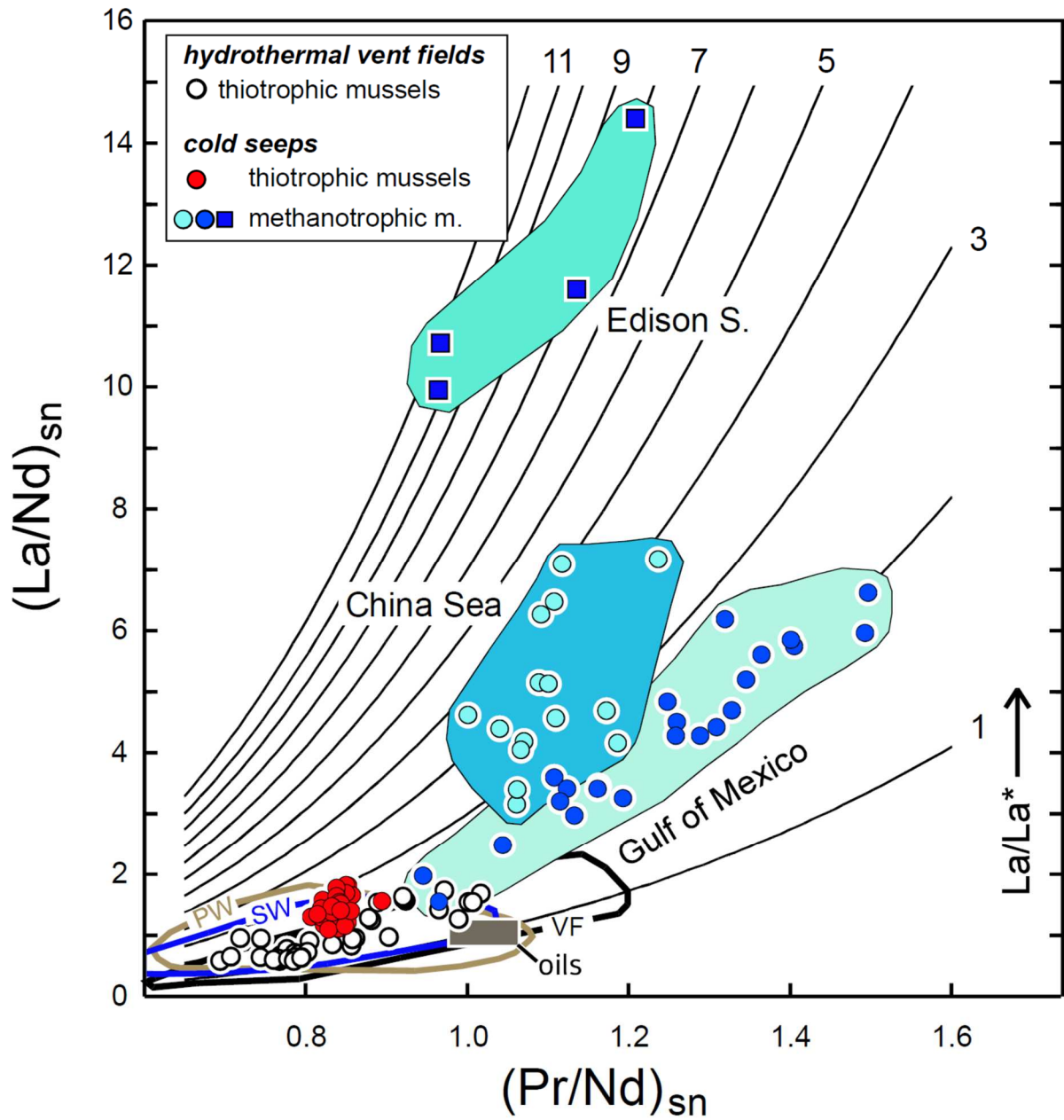
738
 739
 740
 741
 742
 743
 744
 745

Figure 7. Histograms of Sm abundances in mussel shells from hydrothermal vents and cold seeps (data from Bau et al., 2010, Wang et al., 2020, and this study). When two fragments of the same shell were analyzed, we used their average here.



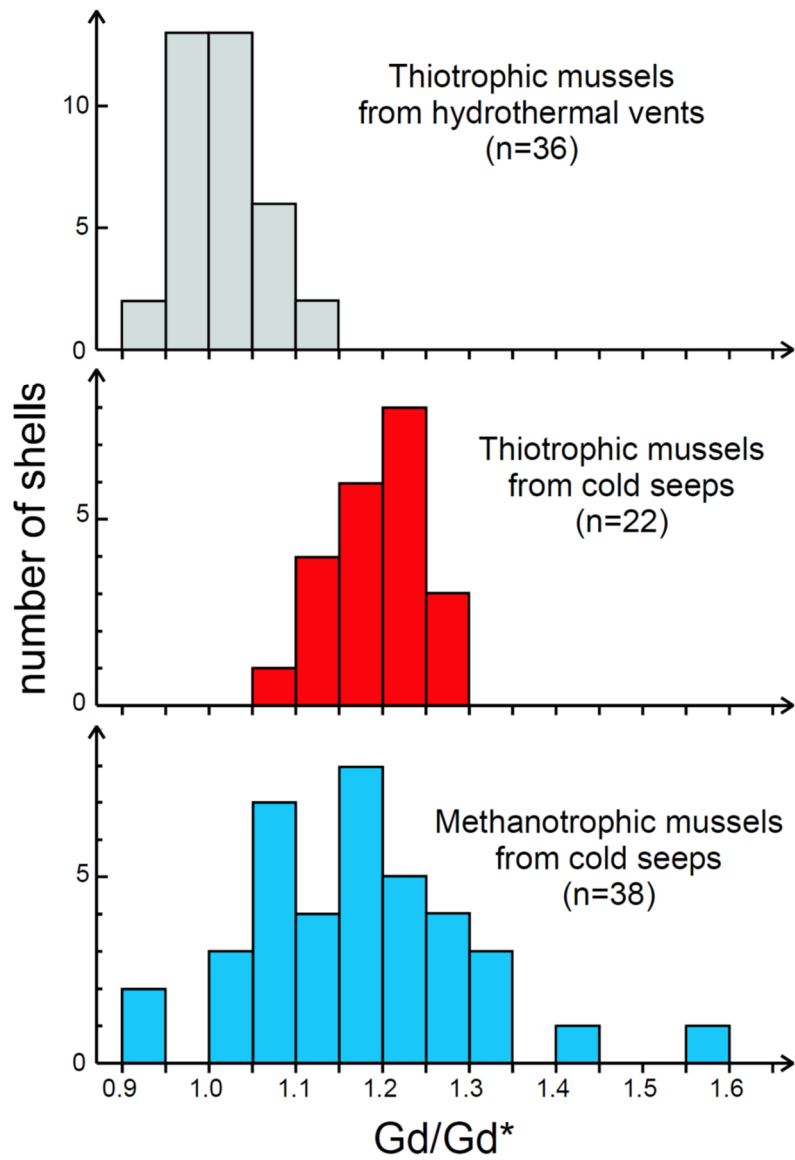
746
 747
 748
 749
 750
 751
 752
 753
 754
 755

Figure 8. $(Tb/Yb)_{sn}$ vs. $(Pr/Sm)_{sn}$ plot for mussels shells (data from Bau et al., 2010, Wang et al., 2020, and this study). Fields for seawater (SW), pore waters (PW) and vent fluids (VF) are drawn from a database of results of the literature (see Bayon et al. (2020b) for the references for seawaters and pore waters, and Bau and Dulski (1999, Douville et al. (1999), Schmidt et al. (2007, 2017), Craddock et al. (2010), and Cole et al. (2014) for vent fluids).



756
 757
 758
 759
 760
 761
 762
 763

Figure 9. $(La/Nd)_{sn}$ vs. $(Pr/Nd)_{sn}$ plot for mussels (data from Bau et al., 2010, Wang et al., 2020, and this study). Fields for seawater (SW), pore waters (PW) and vent fluids (VF) are drawn from a database of results of the literature (see figure 8 for the references). Oils from seeps from the southern Gulf of Mexico are shown for comparison (Smrzka et al., 2019).



764
765
766
767
768
769
770

Figure 10. Histograms of Gd/Gd* ratios in mussel shells from hydrothermal vents and cold seeps (data from Bau et al., 2010, Wang et al., 2020, and this study). When two fragments of the same shell were analyzed, we used their average here.